Mars concretion systems. Although the analogue is not a perfect match in every geologic parameter, the mere presence of these spherical haematite concretions implies significant pore volumes of moving subsurface fluids through porous rock.

Haematite is one of the few minerals found on Mars that can be linked directly to water-related processes. Utah haematite concretions are similar to the Mars concretions with spherical morphology, haematite composition, and loose, weathered accumulations. The abundance of quartz in the Utah example could pose challenges for finding spectral matches to the concretions. However, the similarities and differences of the Utah and Mars haematite concretions should stimulate further investigations. The potential role of biomediation in the precipitation of some terrestrial haematite concretions could also hold important clues in the search for life on Mars. Intriguing factors in the Mars system yet to be explored include: spectral comparisons, the source of the iron, the driving mechanism for fluid flow, and other chemical and physical parameters. This Utah analogue presents a model for a fascinating history of fluid flow in the haematite region of Mars. □

Received 18 February; accepted 26 April 2004; doi:10.1038/nature02600.

1. NASA Jet Propulsion Laboratory. *Mars Exploration Rover Mission* ⟨http://marsrovers.jpl.nasa.gov⟩ (February–March 2004).
2. Glotch, T. D. *et al.* Hematite at Meridiani Planum: Detailed spectroscopic observations and testable hypotheses. *Lunar Planet. Sci. Conf. XXXV* [online] Abstr. 2168; ⟨http://www.lpi.usra.edu/meetings/lpsc2004⟩ (2004).
3. Squyres, S. W. *et al.* Initial results from the MER Athena Science investigation at Gusev Crater and Meridiani Planum. *Lunar Planet. Sci. Conf. XXXV* [online] Abstr. 2187, ⟨http://www.lpi.usra.edu/meetings/lpsc2004⟩ (2004).
4. Chan, M. A., Parry, W. T. & Bowman, J. R. Diagenetic hematite and manganese oxides and fault-related fluid flow in Jurassic sandstones, southeastern Utah. *Am. Assoc. Petrol. Geol. Bull.* **84,** 1281–1310 (2000).
5. Chan, M. A. & Parry, W. T. Rainbow of rocks: mysteries of sandstone colors and concretions in Colorado Plateau Canyon Country. (Utah Geological Survey Public Information Service, Salt Lake City, Utah, 2002); ⟨http://www.ugs.state.ut.us/online/pdf/pi-77.pdf⟩.
6. Christensen, P. R., Morris, R. V., Lane, M. D., Bandfield, J. L. & Malin, M. C. Global mapping of Martian hematite mineral deposits: Remnants of water-driven processes on early Mars. *J. Geophys. Res.* **106,** 23873–23885 (2001).
7. Newsom, H. E. *et al.* Paleolakes and impact basins in southern Arabia Terra, including Meridiani Planum: Implications for the formation of hematite deposits on Mars. *J. Geophys. Res.* **108,** doi:10.1029/2002JE001993 (2003).
8. Catling, D. C. & Moore, J. M. The nature of coarse-grained crystalline hematite and its implications for the early environment of Mars. *Icarus* **165,** 277–300 (2003).
9. Hynek, B. M., Arvidson, R. E. & Phillips, R. J. Geological setting and origin of Terra Meridiani hematite deposit on Mars. *J. Geophys. Res.* **107,** doi:10.1029/2002JE001891 (2002).
10. Ormö, J. & Komatsu, G. Hydrocarbon related bleaching of strata and hematite deposition in red beds at Moab, Utah: A possible analogous process that formed bright layers and hematite deposits on Mars. *Lunar Planet. Sci. Conf. XXXIV* [online] Abstr. 1356, ⟨http://www.lpi.usra.edu/meetings/lpsc2003⟩ (2003).
11. Beitler, B., Ormö, J., Komatsu, G., Chan, M. A. & Parry, W. T. Geomorphic and diagenetic analogs to hematite regions on Mars: Examples from Jurassic Sandstones of Southern Utah, USA. *Lunar Planet. Sci. Conf. XXXV* [online] Abstr. 1289, ⟨http://www.lpi.usra.edu/meetings/lpsc2004⟩ (2004).
12. Antonellini, M. & Aydin, A. Effect of faulting on fluid flow in porous sandstones: geometry and spatial distribution. *Am. Assoc. Petrol. Geol. Bull* **79,** 642–671 (1995).
13. Hood, J. W. & Patterson, D. J. *Bedrock Aquifers in the Northern San Rafael Swell Area, Utah, with Special Emphasis on the Navajo Sandstone.* Technical Publication 78 (Utah Department of National Research, 1984).
14. Chan, M. A., Parry, W. T., Petersen, E. U. & Hall, C. M. ^{40}Ar-^{39}Ar age and chemistry of manganese mineralization in the Moab to Lisbon fault systems, southeastern Utah. *Geology* **29,** 331–334 (2001).
15. Beitler, B., Parry, W. T. & Chan, M. A. Bleaching of Jurassic Navajo Sandstone on Colorado Plateau Laramide Highs: Evidence of exhumed hydrocarbon supergiants? *Geology* **31,** 1041–1044 (2003).
16. Parry, W. T., Chan, M. A. & Beitler, B. Chemical bleaching indicates fluid flow in sandstone deformation bands. *Am. Assoc. Petrol. Geol. Bull.* **88,** 175–191 (2004).
17. Beitler, B., Chan, M. A. & Parry, W. T. Field mapping and multispectral analysis of Jurassic Navajo Sandstone color and iron mineralization, Grand Staircase-Escalante National Monument, Utah. *Geol. Soc. Am. Abstr.* **34,** 277 (2002).
18. Ortoleva, P. T. *Geochemical Self-Organization* (Oxford Univ. Press, 1994).
19. Cornell, R. M. & Schwertmann, U. The iron oxides: Structures, properties, reactions, occurrences and uses. (VCH, New York, 1996).
20. Adamovic, J. in *Ironstones Pseudokarst Reports 2* (eds Adamovic, J. & Cilek, V.) 7–40 (Czech Speleological Society, Zlaty Kun, Prague, 2002).
21. Nuccio, V. F. & Condon, S. M. Burial and thermal history of the Paradox Basin, Utah and Colorado, and petroleum potential of the middle Pennsylvanian Paradox Formation. *US Geol. Surv. Bull.* **76,** O1–O41 (1996).
22. Morgan, P. & Gosnold, W. D. in *Geophysical Framework of the Continental United States* (eds Pakiser, L. C. & Mooney, W. D.) 493–522 (Geological Society of America Memoirs Vol. 172, Boulder, Colorado, 1989).
23. Minitti, M. E., Lane, M. D. & Bishop, J. L. A new hematite formation mechanism for Mars. *Lunar Planet. Sci. Conf. XXXV* [online] Abstr. 1999, ⟨http://www.lpi.usra.edu/meetings/lpsc2004⟩ (2004).
24. Hoffman, N. White Mars: A new model for Mars' surface and atmosphere based on CO_2. *Icarus* **146,** 326–342 (2000).
25. Fernández-Remolar, D. *et al.* The Tinto River, an extreme acidic environment under control of iron, as an analog of the Terra Meridiani hematite site of Mars. *Planet. Space Sci.* **53,** 239–248 (2004).

Acknowledgements We thank the donors of the American Chemical Society Petroleum Research Fund, and the Bureau of Land Management-Grand Staircase Escalante National Monument for partial support of this research (to M.A.C. and W.T.P.). The work by J.O. was supported by the Spanish Ministry for Science and Technology and the Ramon y Cajal Program. The work by G.K. was supported by funding from the Italian Space Agency.

Competing interests statement The authors declare that they have no competing financial interests.

Correspondence and requests for materials should be addressed to M.A.C. (machan@mines.utah.edu).

Deterministic quantum teleportation with atoms

M. Riebe[1], H. Häffner[1], C. F. Roos[1], W. Hänsel[1], J. Benhelm[1], G. P. T. Lancaster[1], T. W. Körber[1], C. Becher[1], F. Schmidt-Kaler[1], D. F. V. James[2] & R. Blatt[1,3]

[1]*Institut für Experimentalphysik, Universität Innsbruck, Technikerstraße 25, A-6020 Innsbruck, Austria*
[2]*Theoretical Division T-4, Los Alamos National Laboratory, Los Alamos NM 87545, USA*
[3]*Institut für Quantenoptik und Quanteninformation, Österreichische Akademie der Wissenschaften, Technikerstraße 25, A-6020 Innsbruck, Austria*

Teleportation of a quantum state encompasses the complete transfer of information from one particle to another. The complete specification of the quantum state of a system generally requires an infinite amount of information, even for simple two-level systems (qubits). Moreover, the principles of quantum mechanics dictate that any measurement on a system immediately alters its state, while yielding at most one bit of information. The transfer of a state from one system to another (by performing measurements on the first and operations on the second) might therefore appear impossible. However, it has been shown[1] that the entangling properties of quantum mechanics, in combination with classical communication, allow quantum-state teleportation to be performed. Teleportation using pairs of entangled photons has been demonstrated[2–6], but such techniques are probabilistic, requiring post-selection of measured photons. Here, we report deterministic quantum-state teleportation between a pair of trapped calcium ions. Following closely the original proposal[1], we create a highly entangled pair of ions and perform a complete Bell-state measurement involving one ion from this pair and a third source ion. State reconstruction conditioned on this measurement is then performed on the other half of the entangled pair. The measured fidelity is 75%, demonstrating unequivocally the quantum nature of the process.

Teleportation of a state from a source qubit to a target qubit requires three qubits: the sender's source qubit and an ancillary qubit that is maximally entangled with the receiver's target qubit, providing the strong quantum correlation. Once these states have been prepared, a quantum mechanical measurement is performed jointly on the source qubit and the ancilla qubit (specifically, a Bell-state measurement, which projects the two qubits onto a basis of maximally entangled states). In this process, the two qubits are projected onto one of four equally likely outcomes. At the same time, the non-local properties of quantum mechanics cause the target qubit to be projected onto one of four corresponding states,

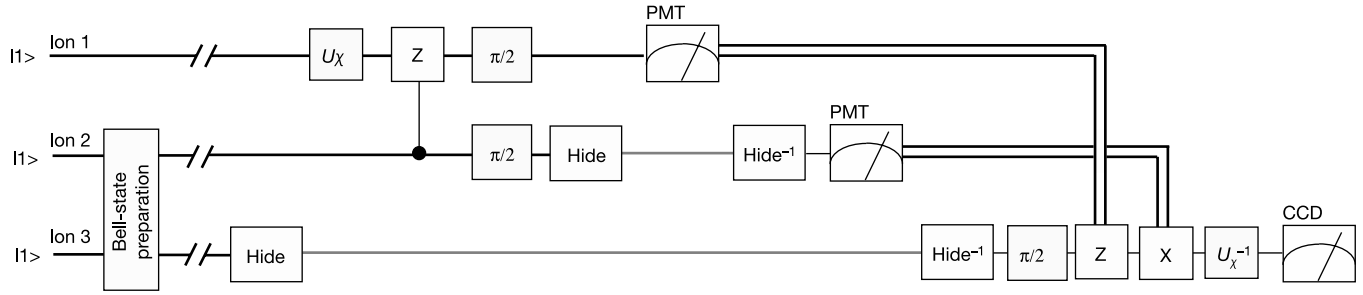

Figure 1 Teleportation from ion 1 to ion 3. A Bell state of ions 2 and 3 is prepared as a resource. The state to be teleported is encoded in ion 1 by the operation U_χ. The Bell-state analyser consists of a controlled Z-gate followed by $\pi/2$ rotations and a state detection of ions 1 and 2. Note that this implementation uses a Bell basis rotated by $\pi/4$ with respect to the standard notation. Therefore a $\pi/2$ rotation on ion 3 is required before the reconstruction operations Z and X. The latter operations are realized by a π rotation around the *z* and *x* axes, respectively. Grey lines indicate qubits that are protected against light scattering. Ions 1 and 2 are detected by observing their fluorescence on a photomultiplier tube (PMT). Only on a detection event $|0\rangle$ is the corresponding reconstruction operation applied to ion 3. Classical information is represented by double lines. For the fidelity analysis we apply U_χ^{-1}, and measure the quantum state of ion 3 by observing its resonance fluorescence using a CCD camera.

each related to the original state of the source qubit, even though no measurement was performed on this qubit. Knowledge of the result of the source-ancilla measurement allows one to choose a simple *a priori* operation to be carried out on the target qubit, resulting in reconstruction of the original quantum state. Because each of the four results on the source-ancilla measurement are equally likely, regardless of the nature of the teleported state, no information about the state is obtained (thus the no-cloning theorem[7] is not violated); further, as classical communication of the measurement outcome is required to complete the state reconstruction, a state cannot be teleported faster than the speed of light. Teleportation does demonstrate a number of fascinating fundamental properties of quantum theory, in particular the non-local property of entangled states, which allows the projective measurement of the source-ancilla pair to create a definite pure state in the target qubit. Furthermore, teleportation has considerable implications for the nascent technology of quantum information processing[8]; besides being a compelling benchmark algorithm for a three-qubit quantum computer, teleportation is a possible primitive for large-scale devices[9].

Experiments demonstrating qubit teleportation[2–6], all of which used photons, were lacking the ability to perform a complete two-photon Bell-state measurement. Successful teleportation events were established by selecting the data after completion of the experiment, searching for the subset of experiments in which the outcome of the measurement and a preset reconstruction operation were matched: that is, teleportation was performed post-selectively. One experiment[10] demonstrated unconditional teleportation of continuous variables, in this case the quadrature amplitudes of a light field. Mention should be made of a liquid-state NMR experiment[11] in which an ensemble of molecules was used in a highly mixed state.

Our implementation of quantum teleportation uses entangled states of massive particles (see also ref. 12). For this, we store three $^{40}Ca^+$ ions in a linear Paul trap; for a detailed description of the experimental set-up, see ref. 13. The ions are arrayed in a linear crystal with an inter-ion distance of 5 μm. A qubit is encoded in a superposition of the $S_{1/2}$ ground state and the metastable $D_{5/2}$ state (lifetime $\tau \approx 1.16$ s) of a $^{40}Ca^+$ ion. Each qubit can be individually manipulated by a series of laser pulses on the $|1\rangle \equiv S_{1/2}(m_J = -1/2)$ to $|0\rangle \equiv D_{5/2}(m_J = -1/2)$ quadrupole transition near 729 nm employing narrow-band laser radiation tightly focused onto individual ions in the string. The qubits are initialized in $|1\rangle$ by optical pumping. The centre-of-mass vibrational mode ($\omega = 2\pi \times 1.2$ MHz) of the ion string is cooled to the ground state as required for controlled interaction between the ions[13].

We teleport the quantum state of ion 1 (the source qubit) onto ion 3 (the target qubit) using the quantum circuit shown in Fig. 1. The sequence is formally equivalent to the one proposed by Bennett *et al.*[1], but adapted to the ion-based quantum processor. As a first step we prepare ion 2 (the ancilla) and 3 in the Bell state $|\psi_+\rangle_{23} = (|0\rangle_2|1\rangle_3 + |1\rangle_2|0\rangle_3)/\sqrt{2}$, the lifetime of which exceeds 100 ms

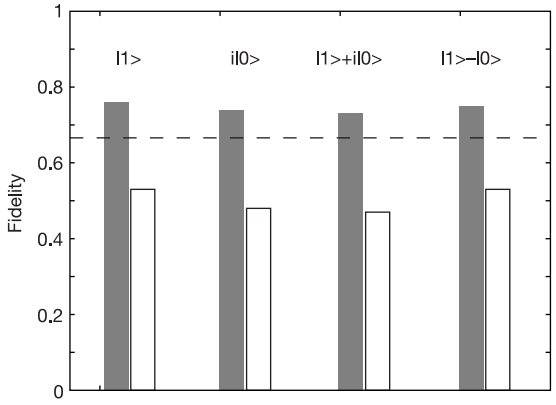

Figure 2 Result of the teleportation. The four test states are teleported with fidelities of 76%, 74%, 73% and 75%, respectively (grey bars). For each input state, 300 single teleportation experiments were performed. The error of each entry, estimated from quantum projection noise, is 2.5%. For comparison, white bars show the results if the reconstruction operations are omitted, yielding an average fidelity of 49.6%. The optimum 'teleportation' obtainable by purely classical means reaches a fidelity of 66.7% (dashed line).

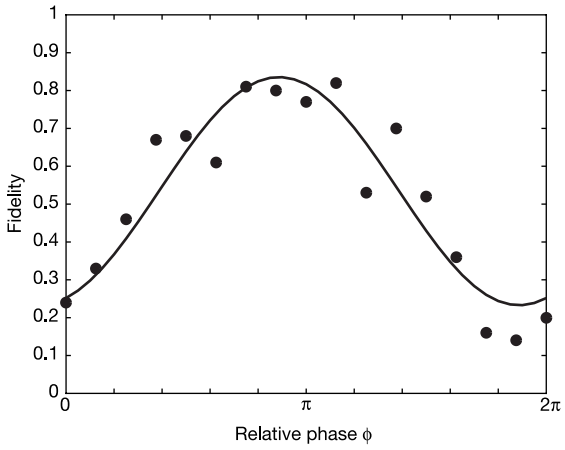

Figure 3 Fidelity of teleportation as a function of the relative phase ϕ of the reconstruction and analysing pulses (see Table 1). This is demonstrated for the test input state $|1\rangle$. Varying ϕ is used for optimizing the experimental fidelity thus accounting for a residual uncompensated phase drift during the entire process (which is the same for all input states).

(ref. 14). Then, at any time within this lifetime, the actual teleportation step—taking less than 2 ms—can be carried out: Ion 1 is prepared in an arbitrary input state with local rotations. In our experiments the teleported state $|\chi\rangle$ was one of a set of four non-orthogonal test states $|\chi^{(1)}\rangle = |1\rangle$, $|\chi^{(2)}\rangle = |0\rangle$, $|\chi^{(3)}\rangle = (|0\rangle + |1\rangle)/\sqrt{2}$ and $|\chi^{(4)}\rangle = (i|0\rangle + |1\rangle)/\sqrt{2}$. The Bell-state analysis is implemented by a controlled phase gate between ion 1 and 2 (ref. 11) followed by a $\pi/2$ pulse on each ion. Then the joint quantum state of ions 1 and 2 is measured by illuminating them with light at 397 nm for 250 μs. Detection of fluorescence indicates the projection of the ion's quantum state into the $S_{1/2}$ state, (logical $|1\rangle$), whereas the absence of fluorescence indicates its projection into the $|0\rangle$ state with nearly 100% detection efficiency. Fluorescence is collected with a photomultiplier tube and the result is stored electronically. The measurement process must preserve the coherence of the target qubit, ion 3. Thus, the state of ion 3 is hidden by transferring it to a superposition of levels that are not affected by the detection light. In Ca^+, an additional Zeeman level $|H\rangle \equiv D_{5/2}(m_J = -5/2)$ can be used for this purpose by moving any $S_{1/2}$ population into the $|H\rangle$ level. The same technique is used to sequentially read out ion 1 and ion 2 and discriminate between all four possible states $\{|0\rangle_1|0\rangle_2, |0\rangle_1|1\rangle_2, |1\rangle_1|0\rangle_2, |1\rangle_1|1\rangle_2\}$. Conditional on the measurement outcome, we apply the appropriate unitary qubit rotation, $-i\sigma_y$, $-i\sigma_z$, $i\sigma_x$ or 1 (with Pauli operators σ_k) to reconstruct the state in the target ion 3, obtaining $|\chi^{(\mathrm{exp})}\rangle$. We emphasize that this conditional, deterministic step, in combination with the complete Bell-state analysis, is one of the crucial improvements with respect to all former experimental realizations of quantum teleportation with qubits. Furthermore, after the teleportation procedure the state $|\chi\rangle$ is always available and may be used for further experiments.

Table 1 **Pulse sequence of the teleportation protocol.**

	Action	Comment
1	Light at 397 nm	Doppler preparation
2	Light at 729 nm	Sideband cooling
3	Light at 397 nm	Optical pumping
Entangle		
4	$R_3^+(\pi/2, 3\pi/2)$	Entangle ion 3 with motional qubit
5	$R_2^C(\pi, 3\pi/2)$	Prepare ion 2 for entanglement
6	$R_2^+(\pi, \pi/2)$	Entangle ion 2 with ion 3
7	Wait for 1 μs – 10,000 μs	Standby for teleportation
8	$R_3^H(\pi, 0)$	Hide target ion
9	$R_1^C(\vartheta_\chi, \varphi_\chi)$	Prepare source ion 1 in state χ
Rotate into Bell basis		
10	$R_2^+(\pi, 3\pi/2)$	Get motional qubit from ion 2
11	$R_1^+(\pi/\sqrt{2}, \pi/2)$	Composite pulse for phasegate
12	$R_1^+(\pi, 0)$	Composite pulse for phasegate
13	$R_1^+(\pi/\sqrt{2}, \pi/2)$	Composite pulse for phasegate
14	$R_1^+(\pi, 0)$	Composite pulse for phasegate
15	$R_1^C(\pi, \pi/2)$	Spin echo on ion 1
16	$R_3^H(\pi, \pi)$	Unhide ion 3 for spin echo
17	$R_3^C(\pi, \pi/2)$	Spin echo on ion 3
18	$R_3^H(\pi, 0)$	Hide ion 3 again
19	$R_2^+(\pi, \pi/2)$	Write motional qubit back to ion 2
20	$R_1^C(\pi/2, 3\pi/2)$	Part of rotation into Bell basis
21	$R_2^C(\pi/2, \pi/2)$	Finalize rotation into Bell basis
Read out		
22	$R_2^H(\pi, 0)$	Hide ion 2
23	PMDetection for 250 μs	Read out of ion 1 with photomultiplier
24	$R_1^H(\pi, 0)$	Hide ion 1
25	$R_2^H(\pi, \pi)$	Unhide ion 2
26	PMDetection for 250 μs	Read out of ion 2 with photomultiplier
27	$R_2^H(\pi, 0)$	Hide ion 2
28	Wait 300 μs	Let system rephase; part of spin echo
29	$R_3^H(\pi, \pi)$	Unhide ion 3
30	$R_3^C(\pi/2, 3\pi/2 + \phi)$	Change basis
Reconstruction		
31	$R_3^C(\pi, \phi)$	$i\sigma_x$ }
32	$R_3^C(\pi, \pi/2 + \phi)$	$-i\sigma_y$ } = $-i\sigma_z$ conditioned on PM detection 1
33	$R_3^C(\pi, \phi)$	$i\sigma_x$ conditioned on PM detection 2
34	$R_3^C(\vartheta_\chi, \varphi_\chi + \pi + \phi)$	Inverse of preparation of χ with offset ϕ
35	Light at 397 nm	Read out of ion 3 with camera

To obtain directly the fidelity of the teleportation, we perform on ion 3 the inverse of the unitary operation $U_\chi \equiv |\chi\rangle\langle 1| + |\bar{\chi}\rangle\langle 0|, (\langle\chi|\bar{\chi}\rangle = 0)$ used to create the input state from state $|1\rangle$. The teleportation is successful if ion 3 is always found in $|1\rangle$. The teleportation fidelity, given by the overlap $F = \langle 1|U_\chi^{-1}\rho_{\mathrm{exp}}U_\chi|1\rangle$, is plotted in Fig. 2 for all four test states. The obtained fidelities range from 73% to 76%. Teleportation based on a completely classical resource instead of a quantum-entangled resource yields[15] a maximal possible average fidelity of 66.7% (dashed line in Fig. 2). Note, however, to rule out hidden variable theories, a fidelity in excess of 0.87 is required[16]. This level of fidelity could be reached by improving primarily the magnetic-field stability and the laser-frequency noise. For comparison, we also show data where the reconstruction pulses were not applied. Without the classical information communicated from the Bell measurement, the receiver's state is maximally mixed, that is there is no information available on the source state. Also, the measurement outcomes of ions 1 and 2 do not contain any information about the initial state $|\chi\rangle$. Indeed, we find each possible result with equal probability of 0.25 ± 0.036, independent of the test input states. Note that only with both the receiver's qubit and the result of the Bell measurement, can the initial state be retrieved.

After the initial Bell-state preparation, only single qubit operations are performed on the target ion (see Fig. 1). Thus, although the scheme presented here takes place in a confining potential common to all three ions, it would, in principle, be possible to separate the target ion from the other two ions. This could be realized in segmented microtrap designs as developed previously[17], which allow separating single ions from a crystal.

To illustrate further the quantum coherence of the teleportation process, we measure its fidelity as a function of the phase of the reconstructing and analysing pulses (see Fig. 3). The oscillation of the teleportation fidelity proves the phase relationship between source and target qubit and thus the quantum nature of the process.

To emphasize the role of the shared entangled pair as a resource, we store the Bell state for some time and then use it only later (after up to 10 ms) for teleportation. For waiting times up to 10 ms (exceeding the time we require for the teleportation by a factor of 5) we observe no decrease in the fidelity. Thus for future quantum-information processing networks, and with entangled states as a resource, quantum teleportation can be used for the distribution of quantum information between different nodes of the network. □

Methods

Pulse sequence

To implement the teleporation we use pulses on carrier transitions $R_i^C(\vartheta, \varphi)$ and $R_i^H(\vartheta, \varphi)$ (no change of the motional state of the ion crystal) and, additionally, on the blue sideband $R_i^+(\vartheta, \varphi)$ (change of the motional state) on ion i. The index C denotes carrier transitions between the two logical eigenstates, and the index H labels the transition from the $S_{1/2}$ ($m_J = -1/2$) to the $D_{5/2}$ ($m_J = -5/2$) level in the Zeeman manifold. For the definitions of $R_i^{C,H,+}(\vartheta, \varphi)$ see refs 13 and 18. In contrast to Fig. 1, in the pulse sequence (Table 1) also the spin-echo pulses[19] are included. These pulses make the algorithm more robust against detunings caused by slow laser and magnetic-field drifts. The timing of these generalized spin-echo pulses was found by optimizing the robustness of the sequence against detunings numerically and experimentally. The conditioned pulses 31,32,33 are applied only if less than six photon detection events were recorded during the respective detection time. For this purpose an electronic circuit counts the pulses of the photomultiplier tube and modifies the pulse sequence accordingly.

Received 17 March; accepted 16 April 2004; doi:10.1038/nature02570.

1. Bennett, C. H. *et al.* Teleporting an unknown quantum state via dual classical and EPR channels. *Phys. Rev. Lett.* **70,** 1895–1899 (1993).
2. Bouwmeester, D. *et al.* Experimental quantum teleportation. *Nature* **390,** 575–579 (1997).
3. Boschi, D., Branca, S., DeMartini, F., Hardy, L. & Popescu, S. Experimental realization of teleporting an unknown pure quantum state via dual classical and Einstein-Podolsky-Rosen channels. *Phys. Rev. Lett.* **80,** 1121–1125 (1998).
4. Pan, J.-W., Daniell, M., Gasparoni, S., Weihs, G. & Zeilinger, A. Experimental demonstration of four-photon entanglement and high-fidelity teleportation. *Phys. Rev. Lett.* **86,** 4435–4438 (2001).
5. Marcikic, I., de Riedmatten, H., Tittel, W., Zbinden, H. & Gisin, N. Long-distance teleportation of qubits at telecommunication wavelengths. *Nature* **421,** 509–513 (2003).
6. Fattal, D., Diamanti, E., Inoue, K. & Yamamoto, Y. Quantum teleportation with a quantum dot single photon source. *Phys. Rev. Lett.* **92,** 037904 (2004).

7. Wootters, W. K. & Zurek, W. H. A single quantum cannot be cloned. *Nature* **299,** 802–803 (1982).
8. Nielsen, M. A. & Chuang, I. J. *Quantum Computation and Quantum Information* (Cambridge Univ. Press, Cambridge, 2000).
9. Gottesman, D. & Chuang, I. L. Demonstrating the viability of universal quantum computation using teleportation and single-qubit operations. *Nature* **402,** 390–393 (1999).
10. Furusawa, A. *et al.* Unconditional quantum teleportation. *Science* **282,** 706–709 (1998).
11. Nielsen, M. A., Knill, E. & Laflamme, R. Complete quantum teleportation using nuclear magnetic resonance. *Nature* **396,** 52–55 (1998).
12. Barrett, M. D. *et al.* Quantum teleportation with atomic qubits. *Nature* (this issue).
13. Schmidt-Kaler, F. *et al.* How to realize a universal quantum gate with trapped ions. *Appl. Phys. B* **77,** 789–796 (2003).
14. Roos, C. F. *et al.* Bell states of atoms with ultra long lifetimes and their tomographic state analysis. *Phys. Rev. Lett.* (in the press) Preprint at ⟨http://arXiv.org/abs/ physics/0307210⟩ (2003).
15. Massar, S. & Popescu, S. Optimal extraction of information from finite quantum ensembles. *Phys. Rev. Lett.* **74,** 1259–1263 (1995).
16. Gisin, N. Nonlocality criteria for quantum teleportation. *Phys. Lett. A* **210,** 157–159 (1996).
17. Kielpinski, D., Monroe, C. & Wineland, D. J. Architecture for a large-scale ion-trap quantum computer. *Nature* **417,** 709–711 (2002).
18. Gulde, S. *et al.* Implementation of the Deutsch-Jozsa algorithm on an ion-trap quantum computer. *Nature* **412,** 48–50 (2003).
19. Hahn, E. L. Spin Echoes. *Phys. Rev.* **80,** 580–594 (1950).

Acknowledgements We thank H. Briegel and P. Zoller for a critical reading of the manuscript. We gratefully acknowledge support by the Austrian Science Fund (FWF), by the European Commission (QUEST, QUBITS and QGATES networks), by the Institut für Quanteninformation, and by the Los Alamos LDRD Program. This material is based upon work supported in part by the US Army Research Office. H.H is funded by the Marie-Curie program of the European Union.

Competing interests statement The authors declare that they have no competing financial interests.

Correspondence and requests for materials should be addressed to R.B. (Rainer.Blatt@uibk.ac.at)

Deterministic quantum teleportation of atomic qubits

M. D. Barrett[1]*, J. Chiaverini[1], T. Schaetz[1], J. Britton[1], W. M. Itano[1], J. D. Jost[1], E. Knill[2], C. Langer[1], D. Leibfried[1], R. Ozeri[1] & D. J. Wineland[1]

[1]*Time and Frequency Division, NIST, Boulder, Colorado 80305, USA*
[2]*Mathematical and Computational Sciences Division, NIST, Boulder, Colorado 80305, USA*

* Present address: Department of Physics, University of Otago, PO Box 56, Dunedin, New Zealand

Quantum teleportation[1] provides a means to transport quantum information efficiently from one location to another, without the physical transfer of the associated quantum-information carrier. This is achieved by using the non-local correlations of previously distributed, entangled quantum bits (qubits). Teleportation is expected to play an integral role in quantum communication[2] and quantum computation[3]. Previous experimental demonstrations have been implemented with optical systems that used both discrete and continuous variables[4–9], and with liquid-state nuclear magnetic resonance[10]. Here we report unconditional teleportation[5] of massive particle qubits using atomic ($^9Be^+$) ions confined in a segmented ion trap, which aids individual qubit addressing. We achieve an average fidelity of 78 per cent, which exceeds the fidelity of any protocol that does not use entanglement[11]. This demonstration is also important because it incorporates most of the techniques necessary for scalable quantum information processing in an ion-trap system[12,13].

Quantum teleportation[1] provides a means for transporting a quantum state between two separated parties, Alice and Bob, through the transmission of a relatively small amount of classical information. For the case of a two-state quantum system or 'qubit', only two bits of classical information are needed, which seems surprising as precise specification of a general qubit state requires an infinite amount of classical information. Aside from the obvious differences in the various experimental demonstrations, the basic teleportation protocol is the same[1]. Alice is in possession of a qubit (here labelled 2) that is in an unknown state $|\psi\rangle_2 \equiv \alpha|\uparrow\rangle_2 + \beta|\downarrow\rangle_2$, where $|\downarrow\rangle$ and $|\uparrow\rangle$ denote eigenstates of the qubit in the measurement basis. In addition, Alice and Bob each possess one qubit of a two-qubit entangled pair that we take to be a singlet $|S\rangle_{1,3} \equiv |\uparrow\rangle_1|\downarrow\rangle_3 - |\downarrow\rangle_1|\uparrow\rangle_3$ (where, for simplicity, we omit normalization factors). Therefore, Alice possesses qubits 1 and 2, while Bob holds qubit 3. Alice wishes to transmit the state of qubit 2 to Bob's qubit using only classical communication. The initial joint state of all three qubits is

$$|\Phi\rangle = |S\rangle_{1,3} \otimes |\psi\rangle_2. \quad (1)$$

This state can be rewritten using an orthonormal basis of Bell states[14] $|\Psi_k\rangle_{1,2} (k = 1–4)$ for the first two qubits and unitary transformations U_k acting on $|\psi\rangle_3 (= \alpha|\uparrow\rangle_3 + \beta|\downarrow\rangle_3)$ so that $|\Phi\rangle = \Sigma_{k=1}^{4} |\Psi_k\rangle_{1,2} (U_k|\psi\rangle_3)$. A measurement in the Bell-state basis $\{|\Psi_k\rangle\}$ by Alice then leaves Bob with one of the four possibilities $U_k|\psi\rangle_3$. Once Bob learns of Alice's measurement outcome (through classical communication), he can recover the original unknown state by applying the appropriate unitary operator, U_k^{-1}, to his state $U_k|\psi\rangle_3$. We note that Alice's Bell-state measurement can be accomplished by transforming from the basis $\{|\Psi_k\rangle_{1,2}\}$ into the measurement basis $\{|\uparrow\uparrow\rangle_{1,2}, |\uparrow\downarrow\rangle_{1,2}, |\downarrow\uparrow\rangle_{1,2}, |\downarrow\downarrow\rangle_{1,2}\}$ before the measurement.

Our implementation uses atomic qubits ($^9Be^+$ ions) that are confined in a linear radiofrequency Paul trap similar to that used in ref. 15. The control electrodes are segmented into eight sections as shown schematically in Fig. 1, providing a total of six trapping zones (centred on electrode segments 2 to 7). Potentials applied to these electrodes can be varied in time to separate ions and move them to different locations. The qubits are composed of the ground-state hyperfine levels $|\uparrow\rangle \equiv |F = 1, m = -1\rangle$ and $|\downarrow\rangle \equiv |F = 2, m = -2\rangle$, which are separated by $\omega_0 \cong 2\pi \times 1.25\,\mathrm{GHz}$. These states are coupled through stimulated Raman transitions[16–18] from two laser

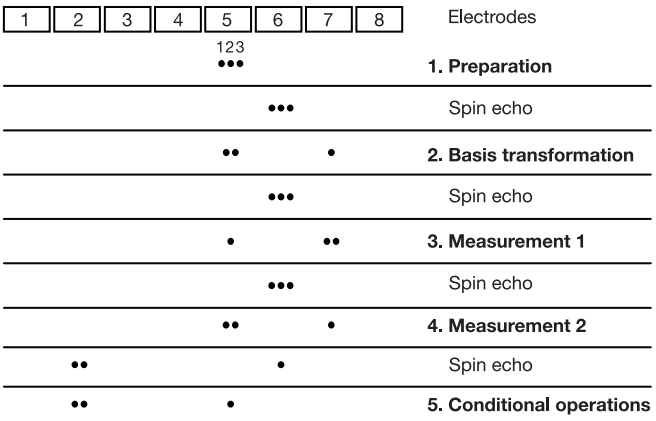

Figure 1 Schematic representation of the teleportation protocol. The ions are numbered left to right, as indicated at the top, and retain their order throughout. Positions, relative to the electrodes, are shown at each step in the protocol. The widths of the electrodes vary, with the width of the separation electrode (6) being the smallest at 100 μm. The spacing between ions in the same trap is about 3 μm, and laser-beam spot sizes (in traps 5 and 6) at the position of the ions are approximately 30 μm. In step 1 we prepare the outer ions in an entangled (singlet) state and the middle ion in an arbitrary state (equation (1)). Steps 2–4 constitute a measurement in a Bell-basis for ions 1 and 2 (Alice's qubits), teleporting the state of ion 2 onto ion 3 (Bob's qubit), up to unitary operations that depend on the measurement outcomes. In step 5 we invoke these conditional operations, recovering the initial state. Interspersed are spin-echo pulses applied in trap 6 that protect the state from de-phasing due to fluctuating magnetic fields but do not affect the teleportation protocol.